Dynamics of magnetized relativistic tori oscillating around black holes

P. J. Montero,[1][*] O. Zanotti,[2] J. A. Font[1] and L. Rezzolla[3,4]

[1]*Departamento de Astronomía y Astrofísica, Universidad de Valencia, Dr Moliner 50, 46100 Burjassot (Valencia), Spain*
[2]*Dipartimento di Astronomia e Scienza dello Spazio, Universita di Firenze, Firenze, Italy*
[3]*Max-Planck-Institut für Gravitationsphysik, Albert-Einstein-Institut, Golm, Germany*
[4]*Department of Physics, Louisiana State University, Baton Rouge, LA 70803, USA*

ABSTRACT

We present a numerical study of the dynamics of magnetized, relativistic, non-self-gravitating, axisymmetric tori orbiting in the background space–times of Schwarzschild and Kerr black holes. The initial models have a constant specific angular momentum and are built with a non-zero toroidal magnetic field component, for which equilibrium configurations have recently been obtained. In this work we extend our previous investigations which dealt with purely hydrodynamical thick discs, and study the dynamics of magnetized tori subject to perturbations which, for the values of the magnetic field strength considered here, trigger quasi-periodic oscillations lasting for tens of orbital periods. Overall, we have found that the dynamics of the magnetized tori analysed is very similar to that found in the corresponding unmagnetized models. The spectral distribution of the eigenfrequencies of oscillation shows the presence of a fundamental p mode and of a series of overtones in a harmonic ratio 2:3: . . . . These simulations, therefore, extend the validity of the model of Rezzolla et al. for explaining the high-frequency QPOs observed in the spectra of low-mass X-ray binaries containing a black hole candidate also to the case of magnetized discs with purely toroidal magnetic field distribution. If sufficiently compact and massive, these oscillations can also lead to the emission of intense gravitational radiation which is potentially detectable for sources within the Galaxy.

Key words: accretion, accretion discs – gravitational waves – hydrodynamics – relativity – stars: oscillations.

1 INTRODUCTION

In a series of recent papers (Rezzolla, Yoshida & Zanotti 2003b; Zanotti, Rezzolla & Font 2003; Zanotti et al. 2005) it has been shown that upon the introduction of perturbations, relativistic tori in equilibrium (or thick accretion discs) manifest a long-term oscillatory behaviour lasting for tens of orbital periods. When the average disc density is close to nuclear matter density, the associated changes in the mass-quadrupole moment make these objects promising sources of high-frequency, detectable gravitational radiation for ground-based interferometers and advanced resonant bar detectors, particularly for Galactic systems. This situation applies to astrophysical thick accretion discs formed following binary neutron star coalescence or the gravitational core collapse of a sufficiently massive star. If the discs are instead composed of low-density material stripped from the secondary star in low-mass X-ray binaries (LMXBs), their oscillations could help explaining the high-frequency quasi-periodic oscillations (QPOs) observed in the spectra of X-ray binaries. Indeed, such QPOs can be explained

in terms of p-mode oscillations of a small-size torus orbiting around a stellar mass black hole (Rezzolla et al. 2003a).

The studies reported in the papers mentioned above have considered both Schwarzschild and Kerr black holes as well as constant and non-constant (power-law) distributions of the specific angular momentum of the discs. However, they have so far been limited to purely hydrodynamical matter models, neglecting a fundamental aspect of such objects, namely the existence of magnetic fields. There is general agreement that magnetic fields are bound to play an important role in the dynamics of accretion discs orbiting around black holes. They can be the source of viscous processes within the disc through magnetohydrodynamic (MHD) turbulence (Shakura & Sunyaev 1973), as confirmed by the presence of the so-called magnetorotational instability (MRI) (Balbus 2003) that regulates the accretion process by transferring angular momentum outwards. In addition, the formation and collimation of the strong relativistic outflows or jets routinely observed in a variety of scales in astrophysics (from microquasars to radiogalaxies and quasars) is closely linked to the presence of magnetic fields.

General relativistic magnetohydrodynamic (GRMHD hereafter) numerical simulations provide the best approach for the investigation of the dynamics of relativistic, magnetized accretion discs

[*]E-mail: pedro.montero@uv.es

under generic non-linear conditions. In recent years there have been important breakthroughs and a sustained level of activity in the modelling of such systems, as formulations of the GRMHD equations in forms suitable for numerical work have become available. This has been naturally followed by their implementation in state-of-the-art numerical codes developed by a number of groups (De Villiers & Hawley 2003; Gammie, McKinney & Tóth 2003; Anninos, Fragile & Salmonson 2005; Duez et al. 2005; Fragile 2005; Komissarov 2005; Shibata & Sekiguchi 2005; Antón et al. 2006; McKinney 2006; Mizuno et al. 2006; Giacomazzo & Rezzolla 2007) many of which have been applied to the investigation of issues such as the MRI in accretion discs and jet formation. Moreover, very recently Komissarov (2006) has derived an analytic solution for an axisymmetric, stationary torus with constant distribution of specific angular momentum and a toroidal magnetic field configuration that generalizes to the relativistic regime a previous Newtonian solution found by Okada, Fukue & Matsumoto (1989). Such equilibrium solution can be used not only as a test for GRMHD codes in strong gravity, but also as initial data for numerical studies of the dynamics of magnetized tori when subject to small perturbations. The latter is, indeed, the main purpose of the present paper.

In this way we aim at investigating if and how the dynamics of such objects changes when the influence of a toroidal magnetic field is taken into account. We discuss the implications of our findings on the QPOs observed in LMXBs with a black hole candidate, assessing the validity of the model proposed by Rezzolla et al. (2003a) in a more general context.

The paper is organized as follows. In Section 2 we briefly review the equilibrium solution found by Komissarov (2006) for a stationary torus with a toroidal magnetic field orbiting around a black hole. The mathematical framework we use for the formulation of the GRMHD equations and for their implementation in our numerical code is discussed in Section 3, while in Section 4 we describe the approach we follow for the numerical solution of the GRMHD equations. Section 5 is devoted to the discussion of the initial models considered, with the results being presented in Section 6. Finally, Section 7 summarizes the paper and our main findings. We adopt a geometrized system of units extended to electromagnetic quantities by setting $G = c = \epsilon_0 = 1$, where ϵ_0 is the vacuum permittivity. Greek indices run from 0 to 3 and Latin indices from 1 to 3.

2 STATIONARY FLUID CONFIGURATIONS WITH A TOROIDAL MAGNETIC FIELD

The initial configurations we consider can be considered as the MHD extensions to the stationary hydrodynamical solutions of thick discs orbiting around a black hole described by Kozlowski, Jaroszynski & Abramowicz (1978), Abramowicz, Jaroszyński & Sikora (1978) and are built using the analytic solution suggested recently by Komissarov (2006).

The basic equations that are solved to construct such initial models are the continuity equation $\nabla_\mu(\rho u^\mu) = 0$ for the rest-mass density ρ, the conservation of energy–momentum $\nabla_\mu T^{\mu\nu} = 0$ and Maxwell's equation $\nabla_\mu(^*F^{\mu\nu}) = 0$, where the operator ∇_μ is the covariant derivative with respect to the space–time four-metric and $^*F^{\mu\nu}$ is the dual of the Faraday tensor defined as

$$^*F^{\mu\nu} = u^\mu b^\nu - u^\nu b^\mu. \tag{1}$$

In this expression u^μ is the fluid four-velocity and b^μ is the magnetic field measured by an observer comoving with the fluid. As usual in ideal relativistic MHD (i.e. for a plasma having infinite

conductivity), the stress–energy tensor $T^{\mu\nu}$ is expressed as

$$T^{\mu\nu} \equiv (\rho h + b^2)u^\mu u^\nu + \left(p + \frac{b^2}{2}\right)g^{\mu\nu} - b^\mu b^\nu, \tag{2}$$

where $g^{\mu\nu}$ are the metric coefficients, p is the (thermal) pressure, h the specific enthalpy and $b^2 \equiv b^\mu b_\mu$.

The equilibrium equations are then solved to build stationary and axisymmetric fluid configurations with a toroidal magnetic field distribution in the tori and a constant distribution of the specific angular momentum in the equatorial plane. The main difference of our solution with that of Komissarov (2006) is that we employ a polytropic equation of state (EOS) of the form $p = \kappa \rho^\Gamma$ for the fluid, where κ is the polytropic constant and Γ is the adiabatic index. Such an EOS has a well-defined physical meaning and differs from the one used by Komissarov (2006), $p = K\omega^q$, where ω is the fluid enthalpy, and K and q are constants.

By imposing the condition of axisymmetry and stationarity in a spherical coordinate system (i.e. $\partial_\phi = \partial_t = 0$), the hydrostatic equilibrium conditions in the r and θ directions are given by

$$\nabla_i \ln(u_t) - \frac{\Omega \nabla_i \ell}{1 - \Omega\ell} + \frac{\nabla_i p}{w} + \frac{\nabla_i(\mathcal{L}b^2)}{2\mathcal{L}w} = 0, \tag{3}$$

with $i = r, \theta$ and $\mathcal{L}(r, \theta) \equiv g_{t\phi}g_{t\phi} - g_{\phi\phi}g_{tt}$. The angular velocity appearing in (3) is defined as

$$\Omega \equiv \frac{u^\phi}{u^t}, \tag{4}$$

the specific angular momentum is given by

$$\ell \equiv -\frac{u_\phi}{u_t} \tag{5}$$

and the components of the magnetic field are

$$b^\phi = \sqrt{\frac{2p_m}{g_{\phi\phi} + 2\ell_0 g_{t\phi} + \ell_0^2 g_{tt}}}, \tag{6}$$

$$b^t = \ell_0 b^\phi. \tag{7}$$

Following Komissarov (2006), we consider the following EOS for the magnetic pressure $p_m = M\mathcal{L}^{q-1}w^q$, where M and q are constants, and which essentially amounts to confining the magnetic field to the interior of the torus. Using this relation, we can integrate equation (3), which in the case of constant specific angular momentum yields

$$W - W_{in} + \ln\left(1 + \frac{\Gamma K}{\Gamma - 1}\rho^{\Gamma-1}\right) + \frac{q}{q - 1}M(\mathcal{L}w)^{q-1} = 0, \tag{8}$$

where the potential W is defined as $W \equiv \ln|u_t|$. Note that in general there will be two radial locations at which ℓ_0 equals the Keplerian specific angular momentum. The innermost of these radii represents the location of the 'cusp' of the torus, while the outermost the 'centre'. When a magnetic field is present, the position of the centre does not necessarily correspond to that of the pressure maximum, as in the purely hydrodynamical case.

In order to solve equation (3) a number of parameters are needed to define the initial model, namely, $\kappa, \Gamma, q, \ell_0, W_{in}$ and the ratio of the magnetic-to-gas pressure at the centre of the torus, $\beta_c = (p_m/p)_c$. Thus, using the definition of β_c, we obtain the rest-mass density at the centre of the torus from the following expression:

$$W_c - W_{in} + \ln\left(1 + \frac{\Gamma}{\Gamma - 1}k\rho_c^{\Gamma-1}\right)$$
$$+ \frac{\beta_c\Gamma}{\Gamma - 1}\left[\frac{1}{1/k\rho_c^{\Gamma-1} + \Gamma/(\Gamma - 1)}\right] = 0. \tag{9}$$

Finally, the equilibrium equation (3) can be solved to obtain the distribution of all relevant MHD quantities inside the torus (Komissarov 2006).

3 GENERAL RELATIVISTIC MHD EQUATIONS

As mentioned in Section 1, there has been intense work in recent years on formulations of the GRMHD equations suitable for numerical approaches (De Villiers & Hawley 2003; Gammie et al. 2003; Anninos et al. 2005; Duez et al. 2005; Komissarov 2005; Shibata & Sekiguchi 2005; Antón et al. 2006; Giacomazzo & Rezzolla 2007). We here follow the approach laid out in Antón et al. (2006) and adopt the $3 + 1$ formulation of general relativity in which the 4D space–time is foliated into a set of non-intersecting space-like hypersurfaces. The $3 + 1$ line element of the metric then reads

$$\mathrm{d}s^2 = -(\alpha^2 - \beta_i\beta^i)\,\mathrm{d}x^0\,\mathrm{d}x^0 + 2\beta_i\,\mathrm{d}x^i\,\mathrm{d}x^0 + \gamma_{ij}\,\mathrm{d}x^i\,\mathrm{d}x^j, \quad (10)$$

where γ_{ij} is the three-metric induced on each space-like slice, and α and β^i are the so-called lapse function and shift vector, respectively.

Under the ideal MHD condition, Maxwell's equations $\nabla^*_\nu F^{\mu\nu} = 0$ reduce to the divergence-free condition for the magnetic field

$$\frac{\partial(\sqrt{\gamma}B^i)}{\partial x^i} = 0, \quad (11)$$

together with the induction equation for the evolution of the magnetic field

$$\frac{1}{\sqrt{\gamma}}\frac{\partial}{\partial t}(\sqrt{\gamma}B^i) = \frac{1}{\sqrt{\gamma}}\frac{\partial}{\partial x^j}\{\sqrt{\gamma}[\alpha\tilde{v}^i B^j - \alpha\tilde{v}^j B^i]\}, \quad (12)$$

where $\gamma \equiv \det(\gamma_{ij})$ and $\tilde{v}^i = v^i - \beta^i/\alpha$, with v^i and B^i being, respectively, the spatial components of the velocity and of the magnetic field, as measured by the Eulerian observer associated to the $3 + 1$ splitting.

Following Antón et al. (2006), the conservation equations for the energy–momentum tensor given by equation (2) together with the continuity equation and the induction equation for the magnetic field can be written as a first-order, flux-conservative, hyperbolic system. The state vector and the vector of fluxes of the fundamental GRMHD system of equations read

$$\frac{1}{\sqrt{-g}}\left(\frac{\partial\sqrt{\gamma}\boldsymbol{F}^0}{\partial x^0} + \frac{\partial\sqrt{-g}\boldsymbol{F}^i}{\partial x^i}\right) = \boldsymbol{S}, \quad (13)$$

where $g \equiv \det(g_{\mu\nu}) = \alpha\sqrt{\gamma}$. The state vector $\boldsymbol{F}^0$ is given by

$$\boldsymbol{F}^0 \equiv \begin{bmatrix} D \\ S_j \\ \tau \\ B^k \end{bmatrix}, \quad (14)$$

with the definitions

$$D \equiv \rho W, \quad (15)$$

$$S_j \equiv \rho(h + b^2/\rho)W^2 v_j - \alpha b^0 b_j, \quad (16)$$

$$\tau \equiv \rho(h + b^2/\rho)W^2 - (p + b^2/2) - \alpha^2(b^0)^2 - D, \quad (17)$$

where W is the Lorentz factor of the fluid. The 'fluxes' $\boldsymbol{F}^i$ in equations (13) have instead explicit components given by

$$\boldsymbol{F}^i \equiv \begin{bmatrix} D\tilde{v}^i \\ S_j\tilde{v}^i + (p + b^2/2)\delta^i_j - b_j B^i/W \\ \tau\tilde{v}^i + (p + b^2/2)v^i - \alpha b^0 B^i/W \\ \tilde{v}^i B^k - \tilde{v}^k B^i \end{bmatrix}, \quad (18)$$

while the 'source' terms $\boldsymbol{S}$ are

$$\boldsymbol{S} \equiv \begin{bmatrix} 0 \\ T^{\mu\nu}(\partial g_{\nu j}/\partial x^\mu - \Gamma^\delta_{\nu\mu}g_{\delta j}) \\ \alpha(T^{\mu 0}\partial\ln\alpha/\partial x^\mu - T^{\mu\nu}\Gamma^0_{\nu\mu}) \\ 0^k \end{bmatrix}, \quad (19)$$

where $0^k \equiv (0, 0, 0)^{\mathrm{T}}$, and $\Gamma^\mu_{\nu\delta}$ are the Christoffel symbols for either a Schwarzschild or Kerr black hole space–time. Note that the following fundamental relations hold between the four components of the magnetic field in the comoving frame, b^μ, and the three vector components B^i measured by the Eulerian observer:

$$b^0 = \frac{W B^i v_i}{\alpha}, \quad (20)$$

$$b^i = \frac{B^i + \alpha b^0 u^i}{W}. \quad (21)$$

Finally, the modulus of the magnetic field can be written as

$$b^2 = \frac{B^2 + \alpha^2(b^0)^2}{W^2}, \quad (22)$$

where $B^2 \equiv B^i B_i$.

Casting the system of evolution equations in flux-conservative, hyperbolic form allows us to take advantage of high-resolution shock-capturing (HRSC) methods for their numerical solution. The hyperbolic structure of those equations and the associated spectral decomposition of the flux-vector Jacobians, needed for their numerical solution with Riemann solvers, is given in Antón et al. (2006).

4 NUMERICAL APPROACH

The numerical code used for the simulations reported in this paper is an extended version of the code presented in Zanotti et al. (2003, 2005) to account for solution of the GRMHD equations. The accuracy of the code has been recently assessed in Antón et al. (2006), with a number of tests including magnetized shock tubes and accretion on to Schwarzschild and Kerr black holes. The system of GRMHD equations (13) is solved using a conservative HRSC scheme based on the HLLE solver, except for the induction equation for which we use the constraint transport method designed by Evans & Hawley (1988) and Ryu et al. (1998). Second-order accuracy in both space and time is achieved by adopting a piecewise-linear cell reconstruction procedure and a second-order, conservative Runge–Kutta scheme, respectively.

The code makes use of polar spherical coordinates in the two spatial dimensions (r, θ) and the computational grid consists of $N_r \times N_\theta$ zones in the radial and angular directions, respectively. The innermost zone of the radial grid is placed at $r_{\min} = r_{\mathrm{horizon}} + 0.1$, and the outer boundary in the radial direction is at a distance about 30 per cent larger than the outer radius of the torus, r_{out}. The radial grid has typically $N_r \simeq 300$ and is built by joining smoothly a first patch which extends from $r_{\min}$ to the outer radius of the torus and is logarithmically spaced (with a maximum radial resolution at the innermost grid zone, $\Delta r/M = 1 \times 10^{-3}$, where M is the mass of the black hole) and a second patch with a uniform grid and which extends up to $r_{\max}$. On the other hand, the angular grid consists of $N_\theta = 100$ equally spaced zones and covers the domain from 0 to π.

As in the hydrodynamical code, a low-density atmosphere is introduced in those parts of the computational domain not occupied by the torus. This is set to follow the spherically symmetric accreting solution described by Michel (1972) in the case that the background

metric is that of a Schwarzschild black hole and a modified solution, which accounts for the rotation of the black hole (Zanotti et al. 2005), when we consider the Kerr background metric. Since this atmosphere is evolved as the rest of the fluid and is essentially stationary but close to the torus, it is sufficient to ensure that its dynamics does not affect that of the torus. This is the case if the maximum density of the atmosphere is five to six orders of magnitude smaller than the central density of the torus. Note that since we limit our analysis to isentropic evolutions of isentropic initial models, the energy equation does not need to be solved. Finally, the boundary conditions adopted are the same as those used by Font & Daigne (2002).

5 INITIAL MODELS

The initial models consist of a number of magnetized relativistic tori which fill their outermost closed equipotential surface, so that their inner radii coincide with the position of the cusp, $r_{in} = r_{cusp}$. In practice, we determine the positions of the cusp and of the maximum rest-mass density in the torus by imposing that the specific angular momentum at these two points coincides with the Keplerian value. Clearly, different values of specific angular momentum will produce tori with different positions of the cusp and of the maximum rest-mass density. In a purely hydrodynamical context, the effect on the dynamics of the tori of the distribution of specific angular momentum, being either constant or satisfying a power law with r, was studied by Zanotti et al. (2003, 2005). In this paper, however, we consider only magnetized tori with constant specific angular momentum as we want to first focus on the influence a magnetic field has on the dynamics, both in a Schwarzschild and in a Kerr background metric. In this way we can conveniently exploit the analytic solution reviewed in Section 2 and which cannot be extended simply to include the case of non-constant specific angular momentum distributions.

Once the specific angular momentum is fixed, the inner edge of the torus r_{in} is determined by the potential gap at such inner edge, $\Delta W_{in} = W_{in} - W_{cusp}$ which, in the case of constant specific angular momentum distributions, is defined as

$$\Delta W_{in} = \ln[(-u_t)_{in}] - \ln[(-u_t)_{cusp}], \qquad (23)$$

with $\Delta W_{in} = 0$ corresponding to a torus filling its outermost equipotential surface.

All of the models are built with an adiabatic index $\Gamma = 4/3$ to mimic a degenerate relativistic electron gas, and the polytropic constant κ is fixed such that the torus-to-black hole mass ratio, M_t/M, is roughly 0.1. Since the mass of the torus is at most 10 per cent of that of the black hole, we can neglect the self-gravity of the torus and study the dynamics of such objects in a fixed background space–time (test-fluid approximation). Moreover, the disc-to-hole mass ratio adopted here is in agreement with the one obtained in simulations of unequal mass binary neutron star mergers performed by Shibata, Taniguchi & Uryū (2003) and Shibata & Sekiguchi (2005).

Overall, we have investigated a number of different models for tori orbiting either non-rotating or rotating black holes. In the case of Schwarzschild black holes, the main difference among the models is the strength of the toroidal magnetic field, which is parametrized by the ratio of the magnetic-to-gas pressure at the centre of the disc, $\beta_c \equiv b^2/(2p)$. In the case of Kerr black holes, on the other hand, we report results for tori orbiting around black holes with spins $a = 0.5, 0.7$ and 0.9, while keeping constant the magnetic-to-gas pressure ratio at $\beta_c = 0.01$. A summary of all the models considered is given in Table 1.

The set of models chosen here will serve a double purpose. Being tori with large average densities, they can provide accurate estimates for the gravitational-wave emission triggered by the oscillations. On the other hand, since the ratio among the eigenfrequencies is the astrophysically most relevant quantity and this does not depend on the density, this set of models is also useful for analysing the oscillation properties of the accretion discs in LMXBs. It is also important to note that for tori with $\beta_c > 1$ the initial solution degrades over time as a significant mass is accreted in these cases, with an accretion rate that increases with the strength of the magnetic field. The dependence of the stability of thick discs with the strength of the toroidal magnetic field will be the subject of an accompanying paper (Rezzolla et al., in preparation).

The maximum strength of the magnetic field at the centre, determined by the parameter β_c, can be calculated through equation (6), which also reflects the dependence of the toroidal magnetic field component on the background metric. The initial models considered are such that β_c takes values between 0 and 1, as shown in Table 1. This also fixes the overall strength of the magnetic field, whose maximum values are reported in the tenth column of the same table. The values of the magnetic field strength at the centre for the case of tori around a Schwarzschild black hole range from

Table 1. From left- to right-hand side the columns report the name of the model, the spin of the black hole, a, the specific angular momentum, ℓ_0, the polytropic constant, κ, the inner and outer radius of the torus, r_{in} and r_{out}, the orbital period at the point of maximum rest-mass density, t_{orb}, the maximum rest-mass density, ρ_{max}, the magnetic-to-gas pressure at the maximum of the rest-mass density, β_c, and the maximum magnetic field, B_{max}. For all models the torus-to-hole mass ratio M_t/M is 0.1 ($M = 2.5\ M_{\odot}$) and the adiabatic exponent of the EOS is 4/3.

| Model	a	ℓ_0	κ (CGS)	r_{in}	r_{out}	t_{orb} (ms)	ρ_{max} (CGS)	β_c	B_{max} (G)
S1	0.0	3.80	9.33×10^{13}	4.57	15.88	1.86	1.25×10^{13}	0.00	0.0
S2	0.0	3.80	9.21×10^{13}	4.57	15.88	1.86	1.26×10^{13}	0.01	2.50×10^{15}
S3	0.0	3.80	9.10×10^{13}	4.57	15.88	1.86	1.27×10^{13}	0.02	3.52×10^{15}
S4	0.0	3.80	8.90×10^{13}	4.57	15.88	1.86	1.28×10^{13}	0.04	4.94×10^{15}
S5	0.0	3.80	8.40×10^{13}	4.57	15.88	1.86	1.29×10^{13}	0.10	7.58×10^{15}
S6	0.0	3.80	7.60×10^{13}	4.57	15.88	1.86	1.34×10^{13}	0.20	1.04×10^{16}
S7	0.0	3.80	6.00×10^{13}	4.57	15.88	1.86	1.39×10^{13}	0.50	1.50×10^{16}
S8	0.0	3.80	4.49×10^{13}	4.57	15.88	1.86	1.40×10^{13}	1.00	1.85×10^{16}
K1	0.5	3.30	2.20×10^{14}	3.16	15.65	1.22	1.44×10^{13}	0.01	4.29×10^{15}
K2	0.7	3.00	2.25×10^{14}	2.57	12.07	0.88	2.74×10^{13}	0.01	6.69×10^{15}
K3	0.9	2.60	7.80×10^{14}	1.77	19.25	0.56	1.87×10^{13}	0.01	1.15×10^{16}
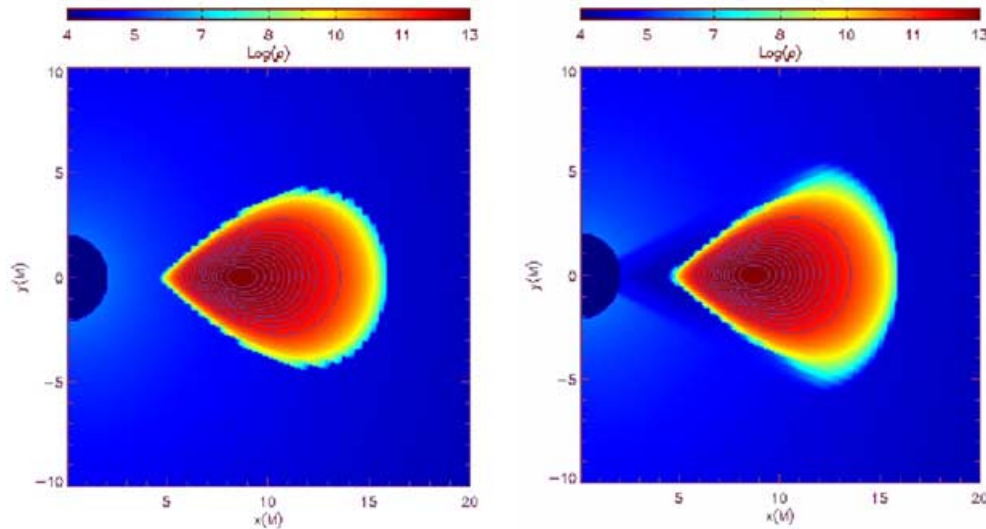
Figure 1. Isocontours of the logarithm of the rest-mass density for the unperturbed model S2. The left-hand panel shows the configuration at the initial time and the right-hand panel the corresponding distribution after 100 orbital time-scales. The equilibrium solution is preserved to high accuracy.

the magnetized model S2 with 2.50×10^{15} G to model S8 with 1.85×10^{16} G. These values are in good agreement with the typical values expected to be present in the astrophysical scenarios that could form a relativistic thick torus, such as the magnetized core collapse (Cerdá-Durán & Font 2006; Obergaulinger, Aloy & Müller 2006; Shibata et al. 2006) and values considered for the collapse of magnetized hypermassive neutron stars by Duez et al. (2006).

In order to trigger the oscillations, we perturb the models reported in Table 1 by adding a small radial velocity (we recall that in equilibrium all velocity components but the azimuthal one are zero). As in our previous work (Zanotti et al. 2003, 2005), this perturbation is parametrized in terms of a dimensionless coefficient η of the spherically symmetric accretion flow on to a black hole (Michel 1972), that is, $v_r = \eta(v_r)_{\text{Michel}}$. In all the simulations reported we choose $\eta = 0.1$, but the results are not sensitive to this choice as long as the oscillations are in a linear regime (i.e. for $\eta \lesssim 0.2$; Zanotti et al. 2003).

Finally, it is worth commenting on the choice made for the magnetic field distribution. On one hand, this choice is motivated by the mere convenience of having an analytic equilibrium solution upon which a perturbation can be introduced. On the other hand, there exists an additional motivation which is more astrophysically motivated. As it has been shown in recent simulations of magnetized core collapse (Cerdá-Durán & Font 2006; Obergaulinger et al. 2006; Shibata et al. 2006) the magnetic field distribution in the nascent, magnetized, protoneutron stars has a dominant toroidal component, quite irrespective of the initial configuration. Since gravitational core collapse is one of the processes through which thick accretion discs may form, the toroidal initial configuration of our simulations is well justified. This choice, however, also has an important consequence. Because of the enforcement of axisymmetry in our 2D simulations and the absence of an initial poloidal magnetic field, in fact, the MRI, which could change even significantly the dynamics of our tori, cannot develop in our simulations. Indeed, Fragile (2005) has investigated the oscillation of an accretion torus having an initial poloidal magnetic field component. Although preliminary, his results suggest that the development of the MRI and of the Papaloizou–Pringle instability (Papaloizou & Pringle 1984) may damp significantly the oscillation modes of accretion tori with

poloidal magnetic fields. We will address this question in a future work.

6 RESULTS

6.1 Oscillation properties

6.1.1 Dynamics of magnetized tori

We have first investigated equilibrium configurations of magnetized tori by performing numerical evolutions of unperturbed tori ($\eta = 0$) and by checking the stationarity of the solution over a time-scale which is a couple of orders of magnitude larger than the dynamical one. As representative example, we show in Fig. 1 the isocontours of the logarithm of the rest-mass density of model S2 as computed at the initial time $t = 0$ (left-hand panel) and at the time when the simulation was stopped (right-hand panel). This corresponds to $t = 100\,t_{\text{orb}}$, where t_{orb} is the Keplerian orbital time for a particle in a circular orbit at the centre of the torus. Aside from the minute accretion of matter from the cusp towards the black hole (see below), the final snapshot of the rest-mass distribution clearly shows the stationarity of the equilibrium initial solution. More precisely, the central rest-mass density, after a short initial transient phase, settles down to a stationary value which differs after 100 orbital time-scales only by 2 per cent from the initial one. This provides a strong evidence of the ability of the code to keep the torus in equilibrium for evolutions much longer than the characteristic dynamical time-scales of these objects.

On the left-hand panel of Fig. 2 we show instead the evolution over $100\,t_{\text{orb}}$ of the central rest-mass density of the least magnetized model S2, when a perturbation with parameter $\eta = 0.1$ is added to the equilibrium model.[1] It is interesting to note that despite the presence of a rather strong toroidal magnetic field, the persistent oscillatory behaviour found in these simulations is very similar to

---

[1] We have here chosen to show the evolution of the rest-mass density as this has a simple physical interpretation, but all of the MHD variables exhibit the same harmonic behaviour.
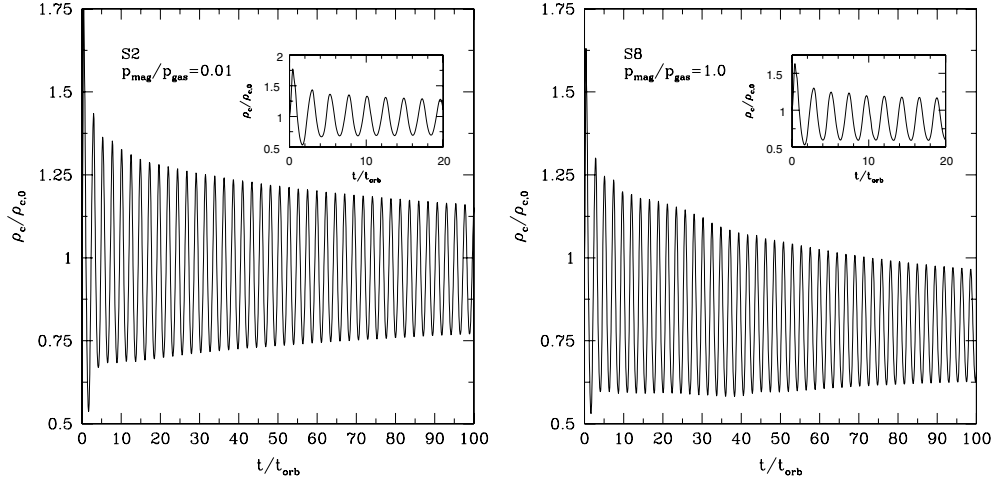
Figure 2. Time evolution of the central rest-mass density normalized to its initial value for models S2 (left-hand panel) and S8 (right-hand panel). Distinctive oscillations are visible during the whole evolution, $t = 100\,t_{\rm orb}$.

the one found in purely hydrodynamical tori (Zanotti et al. 2003, 2005). Note also that the small secular decrease in the oscillation amplitude is not to be related to numerical or physical dissipation, since the code is essentially inviscid and the EOS used is isentropic. Rather, we believe it to be the result of the small but non-zero mass spilled through the cusp at each oscillation (see also discussion below). Furthermore, on a smaller time-scale than the one shown in Fig. 2, the oscillations show a remarkable harmonic behaviour and this is highlighted in the small insets in Fig. 2. This is in stark contrast with the results of Fragile (2005), which were obtained with comparable numerical resolutions, but with an initial poloidal magnetic field configuration. In that case, in fact, the oscillations were rapidly damped in only a few orbital periods.

Results from a representative model with a higher magnetic field are shown in the right-hand panel of Fig. 2, which again reports the evolution of the normalized central rest-mass density for model S8. Note that despite this model has a magnetic-to-gas pressure ratio at the centre $\beta_{\rm c} = 1$, and hence a central magnetic field of $\sim 2 \times 10^{16}$ G, its overall dynamics is very similar to that of model S2. Also in this case, in fact, the oscillations are persistent during the entire evolution ($100\,t_{\rm orb}$) and show almost no damping. However, the amplitude does show variations over time and, most importantly, it no longer maintains a symmetric behaviour between maxima and minima, as a result, we believe, of the increased mass accretion through the cusp. We recall, in fact, that all the initial models considered in our sample correspond to marginally stable tori, that is, tori filling entirely their outermost closed equipotential surface. Any perturbation, however small, will induce some matter to leave the equipotential surface through the cusp, leading to the accretion of mass and angular momentum on to the black hole. Evidence in favour of this is shown in Fig. 3, which reports the accretion mass-flux for model S2 (upper panel) and model S8 (lower panel). While both reflect the oscillations in the dynamics, they also have different mean values, with the one relative to model S8 being almost an order of magnitude larger. Note also the correlation between the fluctuations in the mass-accretion rate and the changes in the oscillation amplitudes shown in Fig. 2. In particular, the sudden change in the mass-flux of model S8 at $t \sim 35\,t_{\rm orb}$ and which corresponds to a change in the amplitude modulation in the right-hand panel of Fig. 2.

Although the accretion-rates are well above the Eddington limit (which is $\sim 10^{-16}\,{\rm M}_\odot\,{\rm s}^{-1}$ for a $2.5\,{\rm M}_\odot$ black hole), the amounts of mass accreted by the black hole at $t = 100\,t_{\rm orb}$ is only 1.3 and
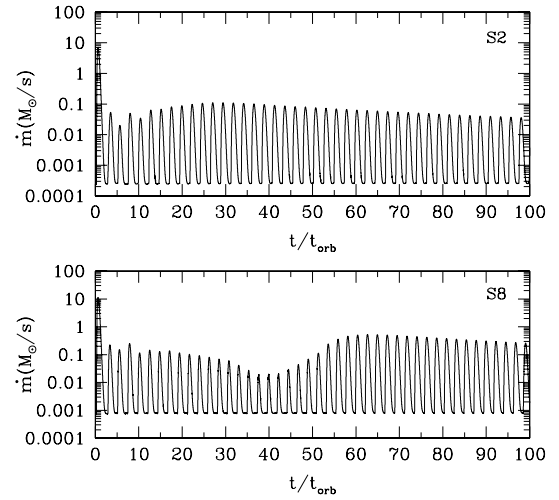

Figure 3. Time evolution of the mass-accretion rate for models S2 and S8.

3.3 per cent of the initial mass for models S2 and S8, respectively. Similarly, the total amount of angular momentum accreted at the end of the simulation would introduce a change in the black hole's spin of less than 1 per cent for both models S2 and S8. Overall, therefore, these changes in the mass and spin of the black holes are extremely small and thus justify the use of a fixed background space–time. Finally, in Fig. 4 we show the evolution of the normalized central rest-mass density for model K2, which corresponds to a torus orbiting around a Kerr black hole with spin $a = 0.7$. Again, a perturbation with parameter $\eta = 0.1$ was added to the equilibrium model so as to investigate the oscillatory behaviour of the torus around its equilibrium position. As in the purely hydrodynamical case, the qualitative behaviour in models around a Kerr black hole is very similar to that found for models around a Schwarzschild black hole, and the dynamics shows, also in this case, a negligible damping of the oscillations after the initial transient.

6.1.2 Power spectra

An important feature of axisymmetric p-mode oscillations of accretion tori is that the lowest order eigenfrequencies appear in
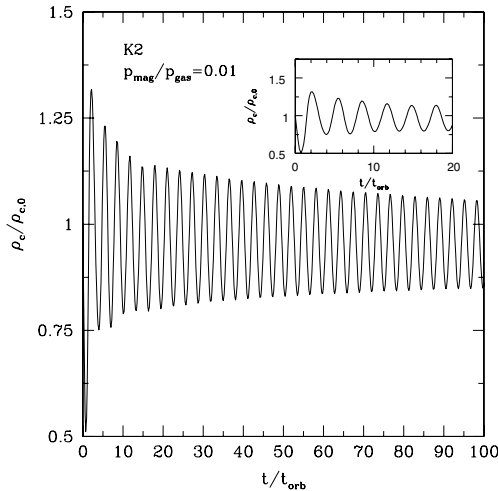
Figure 4. Time evolution of the central rest-mass density normalized to its initial value for the model K2.

the harmonic sequence 2:3. This feature was first discovered in the purely hydrodynamical numerical simulations of Zanotti et al. (2003), subsequently confirmed through a perturbative analysis in a Schwarzschild space–time by Rezzolla et al. (2003b), and later extended to a Kerr space–time and to more general distributions of the specific angular momentum by Zanotti et al. (2005) and Montero, Rezzolla & Yoshida (2004). Overall, it was found that the 2:3 harmonic sequence was present with a variance of ∼10 per cent for tori with a constant distribution of specific angular momentum and with a variance of ∼20 per cent for tori with a power-law distribution of specific angular momentum. Since the 2:3 harmonic sequence is the result of global modes of oscillation, it depends on a number of different elements that contribute to small deviations from an exact relation among integers. The latter, in fact, should be expected only for a perfect 1D cavity, trapping the p modes without losses. In practice, however, factors such as the vertical size of the tori, the black hole spin, the distribution of specific angular momentum, the EOS considered and the presence of a small but non-zero mass-loss, can all influence this departure.

While the understanding of the properties of these modes of oscillation has grown considerably over the last few years (see Montero et al. 2004, for a list of references), and an exhaustive analysis has been made in the case of relativistic slender tori (Blaes, Arras & Fragile 2006), it was not obvious whether such a harmonic sequence would still be present in the case of magnetized discs with toroidal magnetic fields. To address this question, we have performed a Fourier analysis of the time evolution of some representative variables and obtained quantitative information on the quasi-periodic behaviour of the tori. In particular, for all of the models considered, we have Fourier transformed the evolution of the L_2 norm of the rest-mass density, defined as $||\rho||_2 \equiv \sum_{i=1}^{N_r} \sum_{j=1}^{N_\theta} (\rho_{ij})^2$ and studied the properties of resulting power spectra. These, we recall, show distinctive peaks at the frequencies that can be identified with the quasi-normal modes of oscillation of the disc.[2] Clearly, the accuracy in calculating these eigenfrequencies depends linearly on

the length of the time-series and is of 0.01 kHz for the evolutions carried out here and that extend for $100\,t_{orb} \sim 100$ ms.

In Fig. 5 we present the power spectra (PSD) obtained from the L_2 norm of the rest-mass density for model S2 (left-hand panel) and model S8 (right-hand panel); in both panels the solid lines refer to the magnetized tori, while the dashed ones to the unmagnetized counterpart S1, which is shown for reference. A rapid look at the panels in Fig. 5 reveals that the overall dynamics of magnetized tori shows features which are surprisingly similar to those found by Zanotti et al. (2003, 2005) for unmagnetized accretion tori. Namely, the spectra have a fundamental mode f (which is the magnetic equivalent of the p mode discussed in Zanotti et al. (2003, 2005)) and a series of overtones, for which, in particular, the first overtone o_1 can usually be identified clearly. Interestingly, also these spectra show the 2:3 harmonic relation between the frequencies of the fundamental mode and its first overtones. Such a feature remains therefore unmodified and an important signature of the oscillation properties of magnetized tori with a toroidal magnetic field.

It is also worth noting that in the case of mildly magnetized tori, such as model S2, the similarity in the PSD is rather striking and the two spectra differ only in the relative amplitude between the eigenfrequencies o_1, o_2, ... and the modes which are the result of non-linear coupling (e.g. $2f$–o_1, $2f$, ...). On the other hand, in the case of more highly magnetized tori, such as model S8, the magnetic field strength is sufficiently large to produce variations in the eigenfrequencies, which are all shifted to higher frequencies, with deviations, however, which become larger for higher overtones. While not totally unexpected [a magnetic field is known to increase the eigenfrequencies of magnetized stars Nasiri & Sobouti (1989)], these represent the first calculations of the eigenfrequencies of relativistic magnetized discs and, as such, anticipate analogous perturbative studies.

As a way to quantify the differential shift of the eigenfrequencies to larger values, we report in Table 2 the frequencies of the fundamental mode, of the first overtone, and their ratio for all of the models considered. Another analogy worth noticing in the spectra presented in Fig. 5 is the presence of non-linear couplings among the various oscillation modes. These modes were first pointed out by Zanotti et al. (2005) in the investigation of the dynamics of purely hydrodynamical tori with non-constant specific angular momentum in Kerr space–time, and are the consequence of the non-linear coupling among modes, in particular of the f and o_1 modes.

We complete our discussion of the spectral properties of these oscillating discs, by showing in Fig. 6 the PSD for model K2, which, we recall, represents a torus orbiting around a Kerr black hole with spin $a = 0.7$. As for the previous spectra, the dashed line corresponds to the unmagnetized version of model K2 and is included for reference. Overall, the features observed in a Kerr background are very similar to those found for models in the Schwarzschild case. Also in this case, in fact, the fundamental mode, its first overtones and the non-linear harmonics are clearly identified and no evidence appears of new modes related to the presence of a toroidal magnetic field.

As a final remark we note that the 2:3 ratio among the different p modes has a relevance also in a wider context. We recall, in fact, that among the several models proposed to explain the QPOs observed in LMXBs containing a black hole candidate, the one suggested by Rezzolla et al. (2003a) is particularly simple and is based on the single assumption that the accretion disc around the black hole terminates with a sub-Keplerian part, that is, a torus of small size. A key point of this model is the evidence that in these objects the frequencies of the fundamental mode and the first overtone are

---

[2] Note that because of the underlining axisymmetry of our calculations, we cannot compute the effect of transverse hydromagnetic waves, such as Alfvèn waves, propagating along the toroidal magnetic field lines.
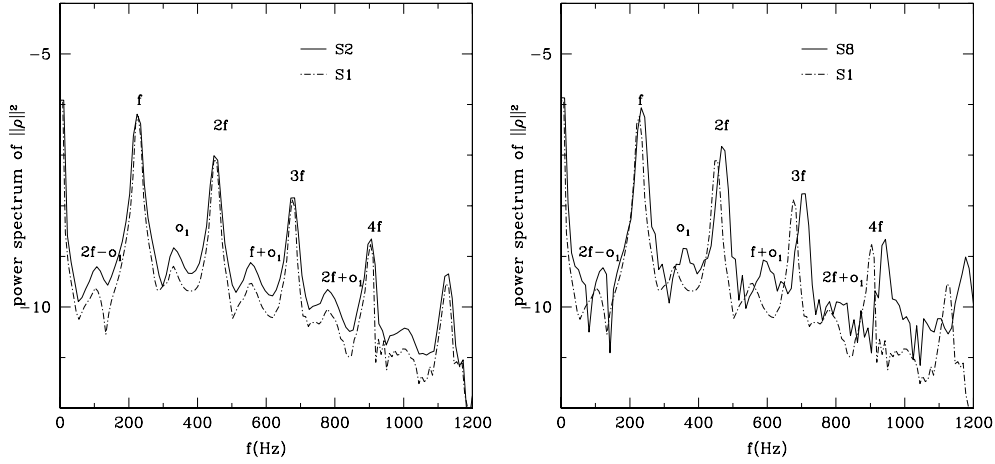
Figure 5. Solid lines: Power spectrum of the L_2 norm of the rest-mass density for models S2 (left-hand panel) and S8 (right-hand panel). The dashed lines show the corresponding PSD for the unmagnetized versions of both models. The units in the vertical axis are arbitrary and the PSDs were obtained using a Hanning filter.

Table 2. From left- to right-hand side, the columns report the name of the model, the frequency of the fundamental mode, the frequency of the first overtone, their ratio and the magnetic-to-gas pressure ratio at the centre of the torus.

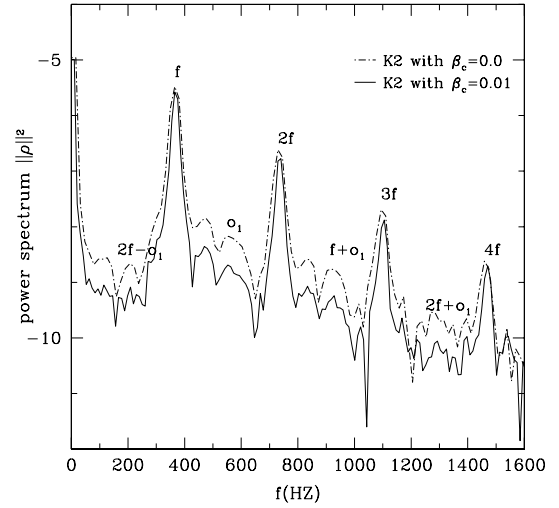| Model	f (Hz)	o_1 (Hz)	o_1/f	β_c
S1	224	332	1.48	0.00
S2	224	332	1.48	0.01
S3	228	336	1.47	0.02
S4	229	333	1.45	0.04
S5	230	330	1.43	0.10
S6	230	340	1.48	0.20
S7	233	345	1.48	0.50
S8	235	341	1.45	1.00
K1	275	418	1.52	0.01
K2	370	560	1.51	0.01
K3	255	404	1.58	0.01

Figure 6. As Fig. 5 but for model K2.

in the 2:3 harmonic sequence in a very wide space of parameter. The simulations presented here further increase this space, extending it also to the case of magnetized tori and thus promoting the validity of this model for QPOs to a more general and realistic scenario. As mentioned above, the simulations presented here refer to tori with a constant distribution of specific angular momentum. However, Montero et al. (2004) and Zanotti et al. (2005) have also shown that the ratio of the o_1 mode to the fundamental one departs only slightly from 3:2 when power-law distributions of the specific angular momentum were considered. Slender tori with a distribution of specific angular momentum close to a Keplerian one, on the other hand, have this ratio much closer to unity (Blaes et al. 2006).

6.2 Gravitational-wave emission

As pointed out by Zanotti et al. (2003) the oscillating behaviour of perturbed accretion tori is responsible for significant changes of their mass-quadrupole moment. As a result, these changes determine the emission of potentially detectable gravitational radiation if the tori are compact and dense enough. This could be the case if the tori are produced via binary neutron star mergers or gravitational collapse of the central core of massive stars. In this section, we extend the

analysis of Zanotti et al. (2003, 2005) for unmagnetized discs and investigate the gravitational-wave emission from constant angular momentum magnetized tori orbiting around black holes.

Although more sophisticated approaches involving perturbative techniques around black holes can be employed to study the gravitational-wave emission from these tori (Nagar et al. 2005; Ferrari, Gualtieri & Rezzolla 2006; Nagar et al. 2007), we here resort to the simpler and less expensive use of the Newtonian quadrupole approximation (Zanotti et al. 2003), which has been suitably modified to account for the presence of a magnetic field, as done by Kotake et al. (2004). In particular, the quadrupole wave amplitude $A_{20}^{\rm E2}$, which is the second time derivative of the mass-quadrupole moment, is computed through the 'stress formula' (Obergaulinger et al. 2006)

$$A_{20}^{\rm E2} = k \int r^2 \mathrm{d}r\mathrm{d}z \left[f_{rr}(3z^2-1) + f_{\theta\theta}(2-3z^2) - f_{\phi\phi} \right.$$
$$\left. - 6z f_{r\theta}\sqrt{1-z^2} - r\rho\frac{\partial\Phi}{\partial r}(3z^2-1) + 3z\rho\frac{\partial\Phi}{\partial\theta}\sqrt{1-z^2} \right],$$
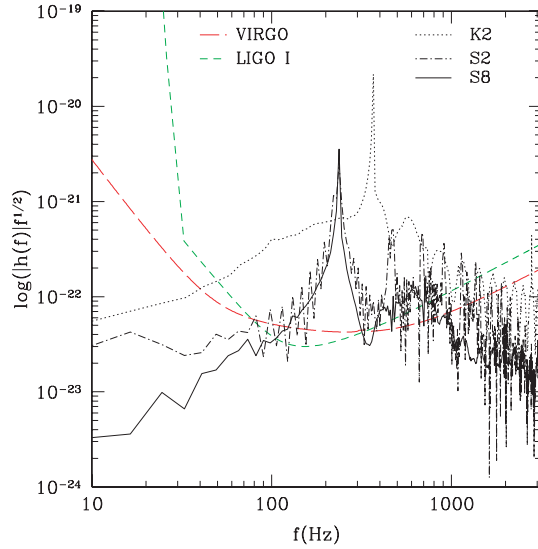$$\tag{24}$$

Figure 7. Comparison between the power spectrum $|h(f)|\sqrt{f}$ of the wave signal for models S2, S8 and K2 and the strain sensitivity of LIGO (dashed line), Virgo (long-dashed line).

where $k = 16\pi^{3/2}/\sqrt{15}$, $z \equiv \cos\theta$, $f_{ij} \equiv \rho v_i v_j - b_i b_j$ and Φ is the gravitational potential, and is approximated at the second post-Newtonian order from the metric function $g_{rr} = 1 - 2\Phi + 2\Phi^2$.

Fig. 7 shows a spectral comparison between the designed strain sensitivity of the gravitational-wave detectors Virgo and LIGO, and the logarithm of the power spectrum $|h(f)|\sqrt{f}$ of the gravitational-wave signals for models S2, S8 and K2 (similar graphs are obtained also for the other models). Note that all of the sensitivity curves displayed in this figure assume an optimally incident wave in position and polarization (as obtained by setting the beam-pattern function of the detector to one), and that the sources are assumed to be located at a distance of 10 kpc.

From Fig. 7 it is clear that all our models lie well above the sensitivity curves of the detectors for Galactic sources and also that there are no significant differences in the power spectra as the magnetic field strength is increased. Interestingly, however, the signal from a torus orbiting around a Kerr black hole is clearly distinguishable from the one around a Schwarzschild black hole. Besides having a fundamental mode at higher frequencies, in fact, also the amplitude is about one order of magnitude larger as a result of it being closer to the horizon and with a comparatively larger central density. As expected from the similarities in the dynamics, the signal-to-noise ratio of these magnetized models is very similar to one of the corresponding unmagnetized tori, and we refer to Zanotti et al. (2005) for a detailed discussion.

7 CONCLUSIONS

We have presented and discussed the results of numerical simulations of the dynamics of magnetized relativistic axisymmetric tori orbiting in the background space–time of either Schwarzschild or Kerr black holes. The tori, which satisfy a polytropic EOS and have a constant distribution of the specific angular momentum, have been built with a purely toroidal magnetic field component. The self-gravity of the discs has been neglected and, as the models considered are all marginally stable to accretion, the minute accretion of mass and angular momentum through the cusp is not sufficient to affect the background black hole metric.

The use of equilibrium solutions for magnetized tori around black holes has allowed us to study their oscillation properties when these are excited through the introduction of small perturbations. In particular, by considering a representative sample of initial models with magnetic field strengths that ranged from 2.5×10^{15} G up to equipartition, and GRMHD evolutions over 100 orbital periods, we have studied the dynamics of these discs and how this is affected by a magnetic field.

Overall, we have found the behaviour of the magnetized tori to be very similar to the one shown by purely hydrodynamical tori (Zanotti et al. 2003, 2005). As in the hydrodynamical case, in fact, the introduction of perturbations triggers QPOs lasting tens of orbital periods, with amplitudes that are modified only slightly by the small loss of matter across the cusp. The enforcement of axisymmetry and the absence of an initial poloidal magnetic field has prevented the development of the MRI, which could influence the oscillation properties and thus alter our conclusions (Fragile 2005). Determining whether this is actually the case will be the focus of a future work, where a more generic magnetic field configuration will be considered.

As for unmagnetized tori, the spectral distribution of the eigenfrequencies shows the presence of a fundamental p mode and of a series of overtones in a harmonic ratio 2:3: . The analogy with purely hydrodynamical simulations extends also to the non-linear harmonics in the spectra and that are the consequence of the non-linear coupling among modes (in particular the f mode and of its first overtone o_1). Also for them we have found a behaviour which is essentially identical to that found in unmagnetized discs. In summary, because of the underlining axisymmetry of our calculations and the use of purely toroidal magnetic fields, we cannot compute the effect of transverse hydromagnetic waves, such as Alfven waves, propagating along the toroidal magnetic field lines. Within this restriction, no new modes have been revealed by our simulations, and in particular no modes which can be associated uniquely to the presence of a magnetic field. Nevertheless, the influence of the magnetic field is evident when considering the absolute values of the eigenfrequencies, which are shifted differentially to higher frequencies as the strength for the magnetic field is increased, with an overall relative change which is ~5 per cent for a magnetic field near equipartition.

Besides confirming the unmagnetized results, the persistence of the 2:3 ratio among the different p modes also has an important consequence. It allows, in fact, to extend to a more general and realistic scenario the validity of the QPO model presented by Rezzolla et al. (2003a) and Schnittman & Rezzolla (2006), and which explains the QPOs observed in the X-ray luminosity of LMXBs containing a black hole candidate with the QPOs of small tori near the black hole. The evidence that this harmonic ratio is preserved even in the presence of toroidal magnetic fields provides the model with additional robustness.

When sufficiently massive and compact, the oscillations of these tori are responsible for an intense emission of gravitational waves and using the Newtonian quadrupole formula, conveniently modified to account for the magnetic terms in the stress–energy tensor, we have computed the gravitational radiation associated with the oscillatory behaviour. Overall, we have found that for Galactic sources these systems could be detected as they lie well within the sensitivity curves of ground-based gravitational-wave interferometers.

As a concluding remark we note that our discussion here has been limited to tori with magnetic fields whose pressure is at most comparable with the gas pressure, that is, $\beta_c \leqslant 1$. The reason behind

this choice is that while in equilibrium, the magnetized tori with a purely toroidal magnetic field are not necessarily stable. Rather, indications coming both perturbative calculations and from non-linear simulations suggest that these tori could be dynamically unstable for sufficiently strong magnetic fields. The results of these investigations will be presented in a forthcoming paper (Rezzolla et al., in preparation).

ACKNOWLEDGMENTS

REFERENCES

Abramowicz M. A., Jaroszyński M., Sikora M., 1978, A&A, 63, 221
Anninos P., Fragile P. C., Salmonson J. D., 2005, ApJ, 635, 723
Antón L., Zanotti O., Miralles J. A., Martí J. M., Ibáñez J. M., Font J. A., Pons J. A., 2006, ApJ, 637, 296
Balbus S. A., 2003, Ann. Rev. Astron. Astrophys., 41, 555
Blaes O. M., Arras P., Fragile P. C., 2006, MNRAS, 369, 1235
Cerdá-Durán P., Font J. A., 2007, Class. Quantum Gravity, in press
De Villiers J., Hawley J. F., 2003, ApJ, 589, 458
Duez M. D., Liu Y. T., Shapiro S. L., Stephens B. C., 2005, Phys. Rev. D, 72, 024028
Duez M. D., Liu Y. T., Shapiro S. L., Shibata M., Stephens B. C., 2006, Phys. Rev. Lett., 96, 031101
Evans C., Hawley J. F., 1988, ApJ, 207, 962
Ferrari V., Gualtieri L., Rezzolla L., 2006, Phys. Rev. D, 73, 124028
Font J. A., Daigne F., 2002, MNRAS, 334, 383
Fragile P. C., 2005, preprint (astro-ph/0503305)
Gammie C. F., McKinney J. C., Tóth G., 2003, ApJ, 589, 444
Giacomazzo B., Rezzolla L. 2007, Class. Quantum Gravity, submitted (gr-qc/0701109)
Komissarov S. S., 2005, MNRAS, 359, 801
Komissarov S. S., 2006, MNRAS, 368, 993
Kotake K., Sawai H., Yamada S., Sato K., 2004, ApJ, 608, 391
Kozlowski M., Jaroszynski M., Abramowicz M. A., 1978, A&A, 63, 209
Landau L. D., Lifshitz E. M., 1976, Mechanics. Pergamon Press, Oxford
McKinney J. C., 2006, MNRAS, 368, 1561
Michel F., 1972, Ap&SS, 15, 153
Mizuno Y., Nishikawa K.-I., Koide S., Hardee P., Fishman G. J., 2006, preprint (astro-ph/0609004)
Mönchmeyer R., Schäfer G., Müller E., Kates R. E., 1991, A&A, 246, 417
Montero P. J., Rezzolla L., Yoshida S'i., 2004, MNRAS, 354, 1040
Nagar A., Font J. A., Zanotti O., De Pietri R., 2005, Phys. Rev. D, 72, 024007
Nagar A., Zanotti O., Font J. A., Rezzolla L., 2007, Phys. Rev. D, 75, 044016
Nasiri S., Sobouti Y., 1989, A&A, 217, 127
Obergaulinger M., Aloy M. A., Müller E., 2006, A&A, 450, 1107
Okada R., Fukue J., Matsumoto R., 1989, PASJ, 41, 133
Papaloizou J. C. E., Pringle J. E., 1984, MNRAS, 208, 721
Rezzolla L., Yoshida S'i., Maccarone T. J., Zanotti O., 2003a, MNRAS, 344, L37
Rezzolla L., Yoshida S'i., Zanotti O., 2003b, MNRAS, 344, 978
Ryu D., Miniati F., Jones T. W., Frank A., 1998, ApJ, 509, 244
Schnittman J. D., Rezzolla L., 2006, ApJ, 637, L113
Shakura N. I., Sunyaev R. A., 1973, A&A, 24, 337
Shibata M., Sekiguchi Y.-I., 2005, Phys. Rev. D, 72, 044014
Shibata M., Taniguchi K., Uryū K., 2003, Phys. Rev. D, 68, 084020
Shibata M., Liu Y. T., Shapiro S. L., Branson C. S., 2006, Phys. Rev. D, 74, 104026
Zanotti O., Rezzolla L., Font J. A., 2003, MNRAS, 341, 832
Zanotti O., Font J. A., Rezzolla L., Montero P. J., 2005, MNRAS, 356, 1372

This paper has been typeset from a TEX/LATEX file prepared by the author.